ORIGINAL

CrossMark

The impact of stack geometry and mean pressure on cold end temperature of stack in thermoacoustic refrigeration systems

Channarong Wantha[1]

Abstract

This paper reports on the experimental and simulation studies of the influence of stack geometries and different mean pressures on the cold end temperature of the stack in the thermoacoustic refrigeration system. The stack geometry was tested, including spiral stack, circular pore stack and pin array stack. The results of this study show that the mean pressure of the gas in the system has a significant impact on the cold end temperature of the stack. The mean pressure of the gas in the system corresponds to thermal penetration depth, which results in a better cold end temperature of the stack. The results also show that the cold end temperature of the pin array stack decreases more than that of the spiral stack and circular pore stack geometry by approximately 63% and 70%, respectively. In addition, the thermal area and viscous area of the stack are analyzed to explain the results of such temperatures of thermoacoustic stacks.

Abbreviations

a	Speed of sound (m s^{-1})
A	Cross-sectional area (m^2)
A_{gas}	Gas cross-sectional area (m^2)
A_{total}	Total cross-sectional area of stack (m^2)
B	Blockage ratio
c_p	Isobaric specific heat (J kg^{-1} K^{-1})
COP	Coefficient of performance
COP_s	Coefficient of performance of the stack
D	Drive ratio
d_o	Diameter (m)
f_k	Thermal Rott function
f_v	Viscous Rott function
H	Enthalpy flux (W)
K	Thermal conductivity (W m^{-1} K^{-1})
L_s	Stack length (m)
L_{sn}	Normalized stack length
l	Half of stack plate thickness (m)
M	Mach number
P_m	Mean pressure (N m^{-2})
P_o	Pressure amplitude (N m^{-2})
Q_c	Cooling power (W)

R	Radius of pore (m)
r_h	Hydraulic radius (m)
r_i	Radius of pin (m)
T_c	Cold end temperature of the stack (^{o}C)
T_h	Hot end temperature of the stack (^{o}C)
T_m	Mean temperature (K)
W	Work flux (W)
x_s	Stack position (m)
x_n	Normalized stack position
y_0	Half of distance between the stack plates (m)
Φ_H	Normalized enthalpy flux
Φ_W	Normalized work flux
δ_k	Thermal penetration depth (m)
δ_{kn}	Normalized thermal penetration depth
δ_v	Viscous penetration depth (m)
ΔT_{mn}	Normalized temperature difference
γ	Ratio of isobaric to isochoric specific heat
σ	Prandtl number
μ	Viscosity (kg m^{-1} s^{-1})
ρ	Density (kg m^{-3})
ω	Angular frequency (rad s^{-1})

✉ Channarong Wantha
  cwantha@rmutt.ac.th

[1] Energy Technology and Heat Transfer Enhancement Laboratory, Department of Agricultural Engineering, Faculty of Engineering, Rajamangala University of Technology Thanyaburi, Thanyaburi, Pathum Thani 12110, Thailand

1 Introduction

The traditional vapor compression system has become the preferred cooling technology at present. However, it has a weakness because the refrigerator's compressor will turn on

and off around the desired temperature to control and maintain a given temperature. This leads to overwork and overconsumption of electrical energy. Furthermore, some systems' refrigerants are still hazardous to the environment. To reduce and eliminate such issues, researchers devote more efforts to the development of alternative cooling technologies. The thermoacoustic refrigeration system is one of the many categories of alternative clean cooling technologies, and can be applied to cooling electronic components, air conditioners for vehicles, refrigerators in an industry or household, and cooling of sensors in space shuttles, etc. [1–3]. In this system, acoustic energy is converted into heat, namely the acoustic power, which has appropriate values of sound amplitude and frequency input to transfer heat from a low to a high temperature medium. Thermoacoustic refrigerators can be driven by either a thermoacoustic heat engine (using a temperature gradient to pump a sound wave) or electrodynamic driver (that converts electrical energy into acoustic power).

The performance of thermoacoustic refrigerators depends on the stack device, which has been confirmed to be the most important component or the heart of a system because it creates the thermoacoustic effect. This effect occurs due to the interaction between the stack plates and gas parcels when the acoustic power is input into the stack. A temperature gradient develops along the stack plates, namely the hot side temperature T_h increases on the ends of stack near locations of the pressure antinode in a standing wave. The cold side temperature T_c occurs on the ends of the stack near the locations of the pressure node. Wetzel, Herman [4] showed that the overall coefficient of performance (COP) of a thermoacoustic refrigerator is the function of the coefficient of performance of stack (COP_s), that is, the maximum of COP_s leads to the maximum of the overall COP of the refrigerator. Therefore, the stack is one of the thermoacoustic components that should be developed for performance first.

Concerning the study of optimum stack device, Tijani et al. [5] studied the design optimization of parallel plate stacks using short stack boundary layer approximation. Zolpakar et al. [6] used the genetic algorithm method to optimize stack device. These studies reported that stack performance depends on the length, position, and spacing of plates. Note that almost all of the experimental and numerical works in the existing literature were focused on thermoacoustic performance using parallel plates or spiral stacks [7–10]. Tijani et al. [11] examined parallel plate stacks with various plate spacings. They found that the optimal plate spacing in the stack is approximately three times the penetration depth values (δ_k). They achieved a cold temperature of −65 °C. Nsofor, Ali [12] studied the performance of thermoacoustic refrigerators with parallel plate stack devices inside resonator tubes. They concluded that the mean pressure of the gas in a system has an effect on temperature differences across the stack. Tasnim et al. [13]

performed numerical studies on operating conditions; the results showed that decreasing the Prandtl number of working fluid in a system should be optimized with stack plate spacing.

However, it isn't only the parallel plate stack geometry that can be used as a device in a thermoacoustic system. Many other possible types of thermoacoustic stacks can be applied, but examination of their effect has not been attempted for the possibility of stack geometries, such as pin arrays, circular pores, and rectangular pores for creating the thermoacoustic process. Swift [1] and Arnott et al. [14] presented the performance of such stack geometries illustrated in terms of Rott's function f. The plot of Rott's function gives the idea of making each stack geometry appropriate. However, in the design of the stack, to achieve the maximum performance, the stack should have a good material property, suitable geometry, and optimal operating parameters to enhance its performance.

Generally, the design of thermoacoustic refrigeration systems requires the maximum cooling load, Q_c or a low temperature T_c on the cold ends of the stack to remove the heat supply from a cold heat exchanger. Thus, the motivation for this work will be to study the effect of three stack geometries, (i.e., parallel plates, circular pores, and pin arrays) and the operating mean pressure on the cold end temperature of the stack. The basic theory of thermoacoustic systems was adopted to fabricate a standing wave thermoacoustic refrigerator as the experimental setup. The computer program DeltaEC was used for the simulation study. The results of the study proposing new knowledge and understanding of stack devices will be helpful in creating a thermoacoustic refrigeration system that can compete with other cooling technologies.

2 Theoretical study

Converting an acoustic oscillation to a temperature gradient along the length of the stack plates in an acoustic field is the main responsibility of stack devices in thermoacoustic systems. The spacing between the plates or pore sizes of the stack is one of the many factors with a significant influence and needs to be optimal to achieve the maximum performance of thermoacoustic stacks. Arnott et al. [14] studied the heat and work flow formulation for a stack with various pore geometries. They found that in an inviscid short stack approximation, the greatest heat and work flows of the stack pores are proportional to the imaginary part of function $F(\lambda)$. Here, $F(\lambda) = 1 - f$ where f is Rott's function. The f-function is known for the description of the pore size of a stack. In this work, three stack geometries were studied in which the equation form of f-functions was expressed as [15].

for parallel plates geometry with a separation of $2y_0 = 2r_h$,

$$f = \frac{\tanh[(1+i)y_0/\delta]}{(1+i)y_0/\delta} \qquad (1)$$

for circular pores of radius $R = 2r_h$,

$$f = \frac{2J_1[(i-1)R/\delta]}{J_0[(i-1)R/\delta](i-1)R/\delta} \qquad (2)$$

and for pin array geometry,

$$f = \frac{-2\alpha_i}{\alpha_o^2 - \alpha_i^2} \frac{Y_1(\alpha_o)J_1(\alpha_i) - J_1(\alpha_o)Y_1(\alpha_i)}{Y_1(\alpha_o)J_o(\alpha_i) - J_1(\alpha_o)Y_0(\alpha_i)} \qquad (3)$$

where $\alpha = (i-1)r/\delta$, J is the Bessel function, Y is the Neumann function, and r_h is the hydraulic radius. Figure 1 plots the results of applying eqs. (1) to (3) by using the Matlab program calculation, which shows the imaginary part of Rott's functions f with the ratio of hydraulic radius to penetration depth (r_h/δ). This graph, using r_h/δ_k, gives f_k and, using r_h/δ_ν, gives f_ν where f_k and f_ν represent the thermal and viscous Rott's functions, respectively. According to Fig. 1, which shows the imaginary part of Rott's function f, the pin stack has the largest negative value of the imaginary part of Rott's function f of all stack geometries. Next to the pin array geometry, the best geometries are parallel plate, and circular pore stack types, respectively. In Fig. 1, the values of Im[$-f_k$] for parallel plate and spiral stack types are maximized when $r_h/\delta_k = 1.1$, and for the circular pores and pin stacks, the maximum value occurs at $r_h/\delta_k = 0.8$ and $r_h/\delta_k = 1.9$, respectively. In this work, these values were used to determine the optimal plate spacing or pore size of the stack device to achieve accuracy in designing it for use as the test device.

From the results of the short stack boundary layer approximation theory, the cooling power and acoustic power equation was developed to estimate and optimize thermoacoustic stack performance. When applied to the dimensionless parameter group, these equation yield
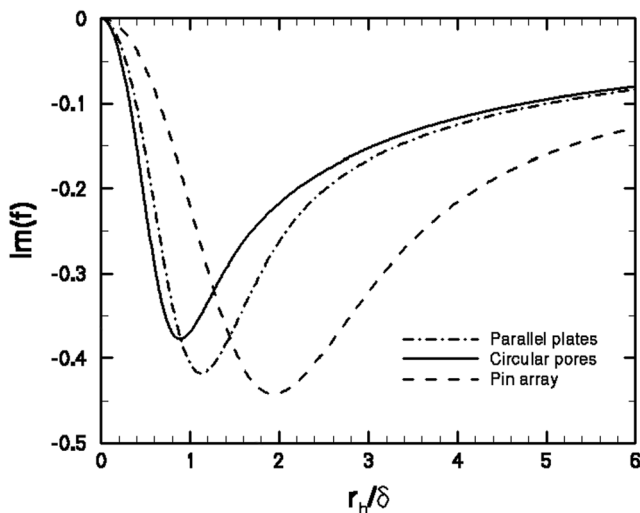

Fig. 1 Imaginary part of Rott functions for different geometries

simplified equations for normalized enthalpy flux, $\Phi_H = H/AP_m a$, and normalized work flux, $\Phi_W = W/AP_m a$, is given as [5, 4]:

$$\Phi_H = \frac{-\delta_{kn}D^2}{4\gamma} \left(\frac{\sin(x_n)\cos(x_n)}{(1+\sigma)\left(1 - \sqrt{\sigma}\delta_{kn} + \frac{1}{2}\sigma\delta_{kn}^2\right)} \right)$$
$$\times \left(\frac{\Delta T_{mn}\tan(x_n)(1+\sqrt{\sigma}+\sigma)}{BL_{sn}(\gamma-1)(1+\sqrt{\sigma})} - \left(1 + \sqrt{\sigma} - \sqrt{\sigma}\delta_{kn}\right) \right) \qquad (4)$$

and,

$$\Phi_W = \frac{\delta_{kn}D^2}{4\gamma} \left\{ \frac{\Delta T_{mn}\tan(x_n)\cos^2(x_n)}{(1+\sqrt{\sigma})\left(1 - \sqrt{\sigma}\delta_{kn} + \frac{1}{2}\sigma\delta_{kn}^2\right)} \right. $$
$$\left. - \left(BL_{sn}(\gamma-1)\cos^2(x_n) + \frac{\sqrt{\sigma}L_{sn}\sin^2(x_n)}{B\left(1 - \sqrt{\sigma}\delta_{kn} + \frac{1}{2}\sigma\delta_{kn}^2\right)} \right) \right\} \qquad (5)$$

where x_n, L_{sn}, B, σ, γ, $\Delta T_{mn} = (T_h - T_c)/T_m$, D, $\delta_{kn} = \delta_k/y_0$ represent, respectively, the normalized stack position, normalized stack length, blockage ratio or porosity of the stack, Prandtl number, ratio of isobaric to isochoric specific heats, normalized stack temperature difference, drive ratio, and normalized thermal penetration (their detailed description is available in Ref [4, 5]). In the present study, eqs. (4) and (5) were rewritten by the conduction terms in the enthalpy flux or cooling power, and the stack heat capacity correction factor ε_s is neglected. The first law of thermodynamics yields an expression for the cooling load of stack in the form

$$\frac{Q_c}{AP_m a} = \frac{|H|}{AP_m a} - \frac{|W|}{AP_m a} \qquad (6)$$

Thus, the performance of the stack was calculated using the expression in terms of the coefficient of performance defined as

$$COP_s = \frac{|\Phi_H| - |\Phi_W|}{|\Phi_W|} = \frac{Q_c/AP_m a}{W/AP_m a} \qquad (7)$$

In considering eqs. (4) and (5), it was found that the equations for both the normalized enthalpy flux and normalized work flux are proportional to term $\delta_{kn}D^2/\gamma$. With this factor, the actual coefficient of performance of the stack, COP_s can thus be optimized independently of the drive ratio D [4]. Considering eq. (6) with (4) and (5), it is found that the square of the driver ratio D^2 has significant effect on the cooling load of the stack (Q_c), i.e., the cooling load, Q_c of the stack can be controlled with the driver ratio.

Consider eq. (6), from which it can be shown that the cooling load, Q_c depends on normalized enthalpy flux, Φ_H,

and normalized work, Φ_W. Thus, the value of Q_c depends on several parameters. However, some of these parameters might be kept constant, such as the blockage ratio B, properties of working fluid such as σ and γ, and the parameters of the stack. Therefore, the remaining factor that is affected by the cooling load, Q_c, of the stack is the speed of sound, drive ratio, and cross-sectional area of the stack. However, the speed of sound in an ideal gas is a function of the mean temperature of the fluid, while the drive ratio, which is defined as the ratio between the dynamic pressure amplitude and the mean pressure (P_o/P_m), will also be a function of the mean pressure of gas in system. Thus, it can be found that the main parameters that have a significant influence on the cooling load Q_c of the thermoacoustic stack are mean pressure, mean temperature, and cross-sectional area of the stack, from which the cooling load Q_c can be expressed as

$$Q_c = Q_c(P_m, T_m, A) \qquad (8)$$

A maximum cooling load of the stack means that in the stack device there is a low temperature T_c on its cold ends. From relevant information in eq. (8), typically, the mean temperature T_m of gas and cross-section area of stack A can be kept constant during the thermoacoustic process. Therefore, the mean temperature and cross-sectional area of stack cancels out from the function of cooling load. Thus, experimental study is performed to examine the effect of the level of gas pressure in a system on the cold end temperature of the stack for different stack geometries, which involves testing with three different stack geometries as already mentioned.

3 Experimental setup and procedure

Two geometries of stacks, spiral, and circular pore stacks, were fabricated for testing using an experimental set-up. The performance of the pin array stack was studied using the simulation program DeltaEC. The design of thermoacoustic stacks is based on the thermoacoustic theory. The pore size or plate spacing of stacks is related to the thermal and viscous penetration depths, expressed respectively as follows:

$$\delta_k = \sqrt{\frac{2K}{\rho c_p \omega}} \qquad (9)$$

and

$$\delta_v = \sqrt{\frac{2\mu}{\rho \omega}} \qquad (10)$$

where K, μ, ρ, c_p, and ω represent, respectively, the thermal conductivity, viscosity, density, specific heat of gas, and angular frequency of sound waves. For this stack design, the

mean pressure of helium gas with 3 bars and a resonance frequency of 720 Hz was selected. The operating frequency of 720 Hz was obtained from simulation using computer program DeltaEC, whose results correspond to the stack length, spacing, location, working fluid, and mean temperature chosen in the study. Additionally, this frequency of 720 Hz is selected based on the stack manufacturability and close to the loudspeaker resonance. The pore size or plate spacing of the stack was obtained by considering the ratio of r_h/δ_k shown in Fig. 1 with eq. (9) and using spacing between the stack plates recommended by Swift [1]. According to the calculations, the results show that the spacing between the plates for the parallel plate stack is $2y_0 = 0.34$ mm and the pore size of the circular pore stack is $2r_h = d_o = 0.32$ mm.

To reach the high temperature difference across the stack, its material must have both a low thermal conductivity and a high heat capacity compared to the working fluid. Thus, Mylar was chosen to build a spiral stack type, and its properties are shown in Table 1. The spiral stack was built by carefully handmade thin Mylar sheets, and the layers were separated by 0.34 mm diameter of fishing line. The spiral stack had a diameter of 80 mm, and its physical length L_s was 63 mm. The fabrication of the circular pore stack geometry is more difficult than that of the spiral geometry, which has not yet been attempted in other literature because a small hollow pore and low thermal conductivity are required. Therefore, in this work, a new methodology was developed to fabricate circular pore stacks to use in testing. Note that the characteristics of electrical cables (see material properties in Table 1) consisted of a copper wire inserted inside of the insulation cover. Therefore, this can be applied for the fabrication of a circular pore stack. All of the copper wires were removed from the insulation cover of the electrical cable to make a hollow circular tube. Then, each electrical insulation cover was gathered without the copper wires, and a circular pore stack was created.

The circular pore stack consists of several electrical insulation covers aligned parallel with the acoustic axis; a pore with an inner diameter of 0.32 mm and an outer diameter of 1.2 mm is used. The circular pore stack geometry has a total diameter of 80 mm, and a length L_s of 63 mm. Figure 2 shows a

Table 1 Stack properties for experiment

Stack properties	Value	
Stack material	Mylar	PVC
Thermal conductivity (W m^{-1} K^{-1})	0.16	0.17
Density (kg m^{-3})	1347.5	1100
Specific heat (J kg^{-1} K^{-1})	1110	900
Blockage ratio	0.538	0.27

Fig. 2 Schematic diagram and photographic view of spiral and circular pore stack geometry used for the experiments

Spiral stack   Circular pore stack
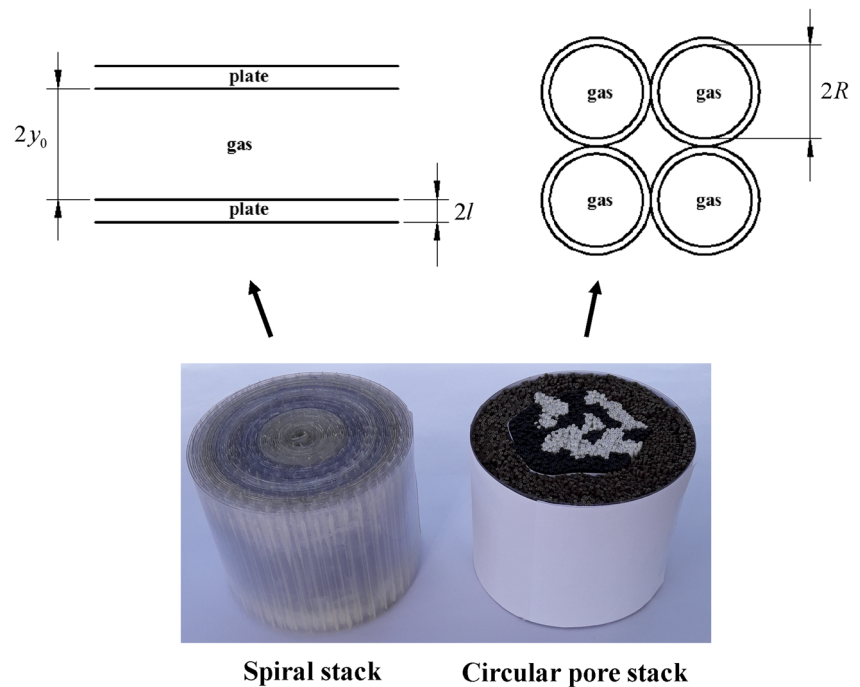
schematic diagram and photographic view of the two stack geometries in this study. The porosity or blockage of the stack is defined as

$$B = \frac{A_{gas}}{A_{total}} \tag{11}$$

Hence, A_{gas} and A_{total} is the cross-sectional area of the gas and total cross-sectional area of the stack, respectively. The value blockage of each stack type is listed in Table 1.

The details of the experimental set-up are schematically illustrated in Fig. 3. The straight resonator was built from a steel tube; the internal tube diameter was 81 mm with a wall thickness of 3.5 mm. It was divided into five portions for easier operation, and an O-ring was used for sealing the gas. The total resonator length is 600 mm, which does not include the loudspeaker housing. One end of the resonator was attached to a 150 W rms commercial loudspeaker to generate sound waves inside the resonator. The other end of the resonator was closed with an end cup (reflector). This study is interested in the temperature difference across the stack only; thus, in the experimental set-up, two heat exchangers were not installed inside the resonator, which means that no thermal reservoirs were attached to the stack and the thermoacoustic heat flow is sustained by the pores themselves. Because the heat exchangers were placed at the hot end and cold end of the stack, they caused a substantial flow blockage and decline in the performance of the stack device, which may cause the results to be misinterpreted. Thermal insulation covers on the resonator tube were therefore used to eliminate thermal leaks during the heat transfer process.

Six thermocouples were used to measure the temperature distribution on the cold and hot ends of the stack. Three thermocouples were installed at the hot end, and the other three thermocouples were installed at the cold end of the stack. All thermocouples' wires were inserted via the feed through the plug inside the resonator to prevent gas leaks. One thermocouple wire was employed to measure the ambient temperature of the resonator tube. All thermocouples in the present study were T-type, and the thermocouple accuracy was ±0.1 °C. The data acquisition board NI-4350 USB via VI Logger software was used to collect the temperature data. One digital pressure gauge was used to measure the gas mean pressure inside the resonator with an accuracy of ±0.01 bar.

The experiments were conducted using the experimental set-up shown in Fig. 3. The loudspeaker was connected to an acoustic power amplifier and a function generator to provide the required acoustic power and frequency inside the resonator. Helium gas was used as a working fluid, and experiments were performed in the range of 1 to 4 bars. The helium gas was charged after a vacuum pump drained the air in the resonator into the surroundings. The mean temperature was set to 305 K. The stack sample used in the study was placed in the resonator at $x_s = 50$mm (see Fig. 3).

The uncertainties in the experimental results was estimated by the following equation, which was described by Holman [16]:

$$u_R = \left[\left(\frac{x_1}{R} \frac{\partial R}{\partial x_1} u_1 \right)^2 + \left(\frac{x_2}{R} \frac{\partial R}{\partial x_2} u_2 \right)^2 + \cdots + \left(\frac{x_n}{R} \frac{\partial R}{\partial x_n} u_n \right)^2 \right]^{1/2} \tag{12}$$

Equation (12) was used to calculate the relative uncertainty in result R that was a given function of the independent

Fig. 3 Schematic diagram of experimental apparatus
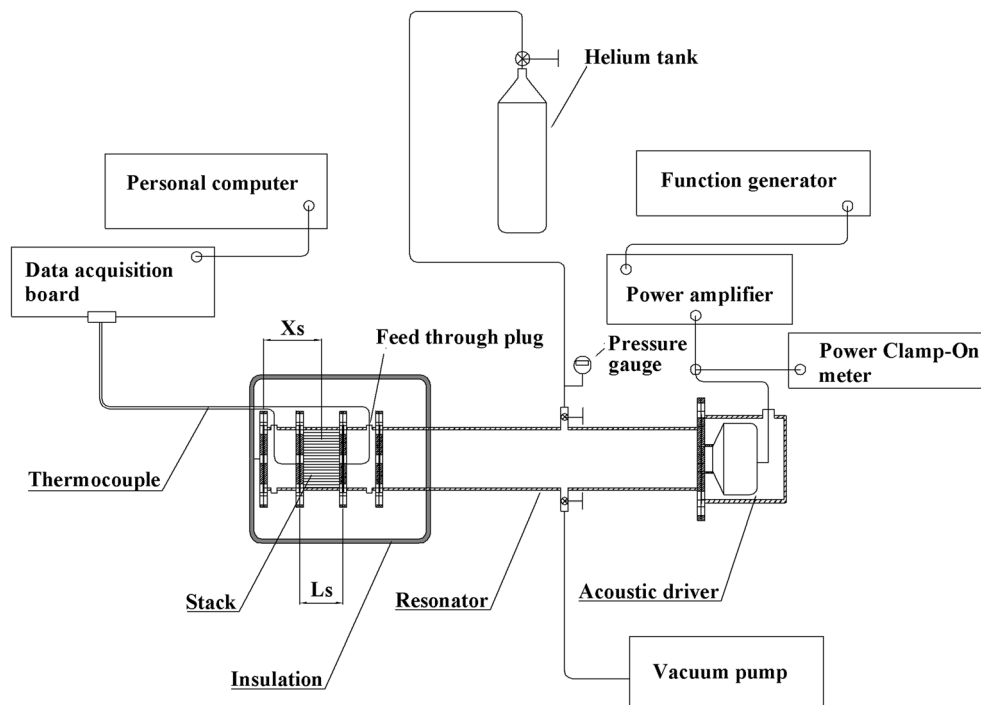
variables $x_1, x_2, \ldots, x_n$, i.e., $R = R(x_1, x_2, \ldots, x_n)$. Accordingly, the experimental uncertainty for the thermocouple was estimated as a maximum relative uncertainty of 1.68%.

4 Results and discussion

Experimental studies were performed to determine the effect of each stack geometry and different mean pressures used on cold-end temperature response of the stack. The operating frequency of the system was independent of the gas mean pressure; therefore, in all cases, the operating frequency of

Fig. 4 Cold end temperature of spiral stack geometry versus time history for different mean pressures

the system was kept constant at 720 Hz. Figure 4 illustrates the history of the cold end temperature of the spiral stack as a function of time when the mean pressure of gas in the system varied. Figure 4 indicated that an increase in mean pressure led to a change in the cold end temperature of the stack and resulted in cooling load, which is in agreement with eq. (8).

Note that for the stack alone in the resonator, at the starting point of the measurement, the cold end temperature of the stack decreased quickly and then rose slowly until a steady state was reached, as the cold end temperature cannot further decrease due to the thermoacoustic mechanism. At the beginning of the system, when there is no temperature gradient on the stack, the thermoacoustic heat flow is high. However, when the temperature gradient is developed and the heat flow in the gas within the stack is balanced, the steady state temperature is reached after a certain time. Also, this phenomenon is in agreement with the experimental results reported in Fig. 5 for the circular pore geometry. Figure 5 shows the history of the temperature at the cold end of the circular pore stack and compared to the spiral stack when the mean pressure was varied. Note that at the same mean pressure, the spiral stack cooled down more quickly than the circular pore stack. The charge mean pressure has less of an impact on the cold end temperature when a system uses a circular pore stack.

The results in Figs. 4 and 5 show that for the range of the mean pressure studied, the value of the cold end temperature is lower with increases in the mean pressure. However, in both the spiral and circular pore stacks, the lowest temperature at the cold end occurred at the same mean pressure is 3 bars, which corresponds to the design
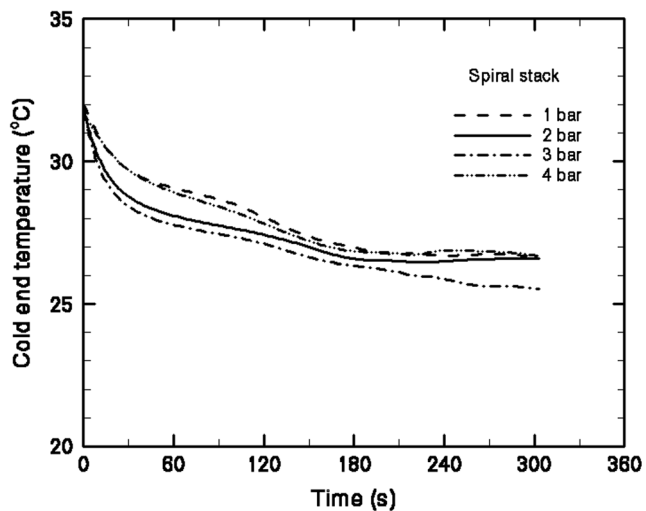
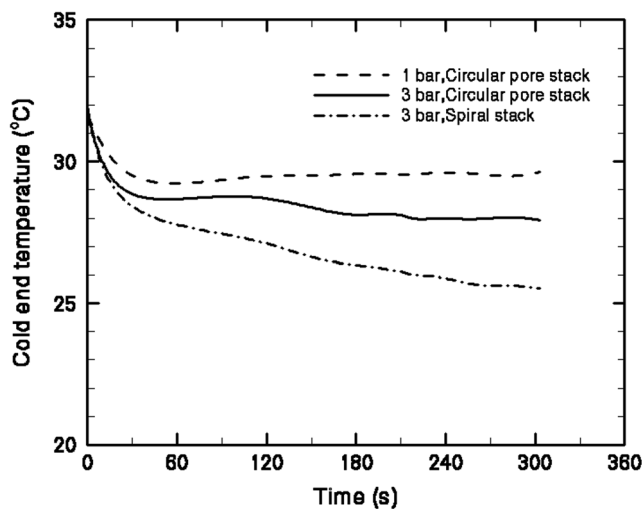Fig. 5 Cold end temperature of circular pore stack geometry versus time history for different mean pressures

Fig. 6 Cold end temperature versus pressure amplitude

condition as mentioned earlier. Increasing the mean pressure of the gas in the system cannot further decrease the cold end temperature. This is because, as the mean pressure increases, the thermal penetration depth δ_k and the pore size or plate spacing of the stack device is small as well. Thus in this present study, this means that a high mean pressure of 4 bars is not better than 3 bars. Therefore, the mean pressure values in the system should correspond with the stack plate spacing or pore size of the hollow stack types. At a mean pressure of 1 bar, the cold end temperature will be reduced to 16.8% for spiral stacks and 7.4% for circular pore stacks compared with the initial temperature. At a mean pressure of 3 bars, the cold end temperature will be reduced to 20.3% for spiral stacks and 12.7% for circular pore stacks compared with the initial temperature.

A low cold end temperature achieved increases in the mean pressure in the system. This is because, as the mean pressure of the system increases at a constant sound speed a, the dynamic pressure amplitude P_o also increases. The dynamic pressure amplitude is related to the equation of the drive ratio D defined as [5]

$$D = \frac{P_o}{P_m} = \frac{M\rho_m a^2}{P_m} \tag{13}$$

Where M is the acoustic Mach number and was limited at $M \approx$ 0.1 for gas as the working fluid [1]. ρ_m is the density of the gas.

Eq. (13) illustrates that a high density of gas, caused by a higher mean pressure of the gas, has a significant effect on both the pressure amplitude and drive ratio. As shown in Fig. 6, the results indicate that a linear behavior is displayed between mean pressure and pressure amplitude, i.e., the higher the mean pressure of the gas in the system, the higher is the dynamic pressure amplitude generated; also, this affects the cold end temperature of
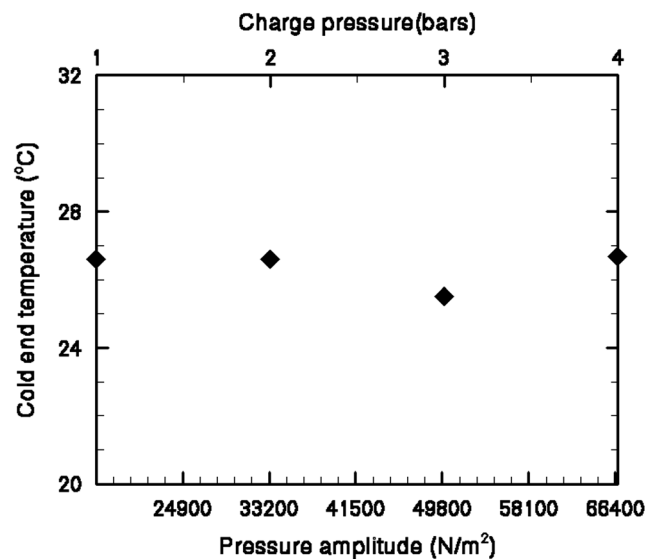
the stack. Thus, for thermoacoustic refrigerators, both the mean pressure and driver ratio can cause the cold end temperature to decrease from the initial temperature.

Figure 7 shows the results of the simulation studies carried out using the DeltaEC simulation software developed by a researcher at the Los Alamos National Laboratory in the United States. Important details for the simulation performed are the use of helium as the working gas and that the material for the pin arrays, circular pores and parallel plates stack geometry are Mylar. The resonator's dimensions and the position of the stack in the resonator were determined according to the experimental set-up design. In the DeltaEC program, the stack segments STKSLAB, STKCIRC, and STKPINS were chosen for the stack geometry for simulation as parallel plates or spiral, circular pore, and pin array stack geometry, respectively. The blockage ratio of parallel plates and circular pores is the same as in the
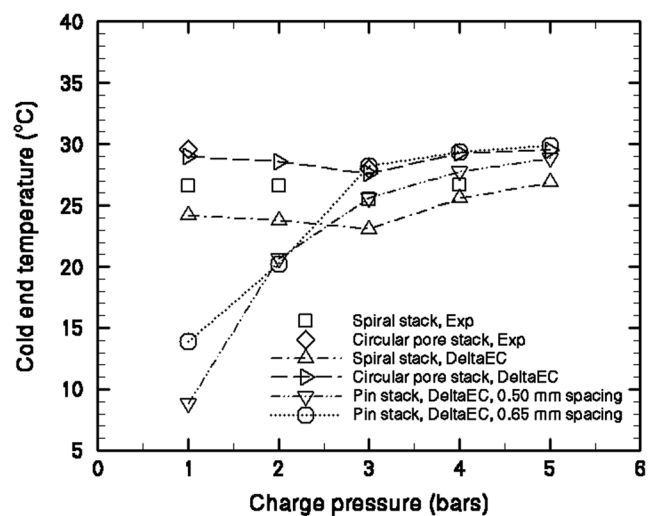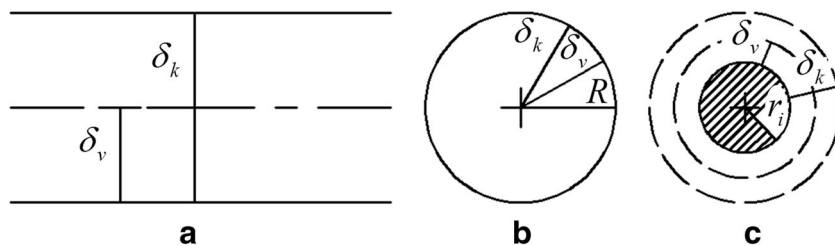

Fig. 7 Experimental and simulated cold end temperature versus mean pressure for different stack geometries

experimental study (see Table 1). In the case of STKPINS for the pin array stack, the input variable of 2y0, which is the center-to-center distance between the nearest-neighbor pins in the hexagonal array of pins, varied between 0.5 and 0.65 mm. The input variable of the R pin in DeltaEC will be set to constant at 0.05 mm. The length of the pin array was calculated as 63 mm. In all cases, during the process of calculation, a hot temperature of 305 K is kept constant.

The focus of the simulation results in the case of the pin array stack is the distance from pin to pin of 0.5 and 0.65 mm spacing. As expected, the mean pressure has an impact on the cold end temperature of the pin array stack. Based on the calculation conditions, the lowest cold end temperature occurred at 1 bar, and any further increase in the mean pressure will result in the temperature at the cold end of the stack to also increase. The pin array stack with a spacing of 0.5 mm is better than that at 0.65 mm, around 36.3% at 1 bar. It is concluded that the spacing between pins should not be too much. The typical spacing between pins in the hexagonal array of pins is between 0.5 to 1.0 mm and a diameter of approximately 0.1 mm [17]. This makes its manufacturing difficult. In the results of the parallel plate or spiral stack, the simulation results indicated that varying the mean pressure has a high impact on the cold end temperature. However, in the case of the circular pore stack, it is observed in Fig. 7 that the influence of the operating mean pressure has a minimal impact on the cold end temperature of the stack; the experiment and calculation give the same results, as shown in Fig. 5.

A comparison of the cold-end temperature of each stack shows that at a low mean pressure of 1 bar, the pin array stack gives a lower cold-end temperature than other geometries. Thus, if the thermoacoustic refrigerator uses a pin array stack as a device, it will have a low cold-end temperature than the spiral stack and circular pore stack geometries by approximately 63% and 70%, respectively, in terms of the cold end temperature of the stack. The reason for the different cold-end temperatures of the stack geometries is due to the results of the ratio of the thermal area to the viscous area of the stack. More thermal penetration depth or thermoacoustic area leads to improved temperature difference of the stack. The ratio of thermal area to viscous area of the stack can be obtained by considering Figs. 8a to c; thus, the ratio of thermal area to viscous area is proportional to (δ_k/δ_v) for the parallel plate, $((R^2 - (R - \delta_k)^2)/(R^2 - (R - \delta_v)^2)$ for the circular pore stack, and $((r_i + \delta_k)^2 - r_i^2)/((r_i + \delta_v)^2 - r_i^2)$ for the pin stack. In the circular pore stack geometry, in only one case was there the

possibility of a radius of $R = \delta_k$, in which the ratio of thermal area to viscous area becomes $\delta_k/\delta_v = 1$. The ratio of the thermal area to viscous area of the pin array stack is $(\delta_k/\delta_v)^2$ if the radius $r_i < \delta_k$. Therefore, from these ratios, it is proposed that pin array stack geometry improves the thermal to viscous areas more than the other geometries. However, if the radius r_i of a pin is too small, the heat capacity of the pins might not be large enough compared to the fluid, and the temperature difference across the stack decreases [1, 18]. In addition, if the pin stack geometry has more spacing between pins, the thermal effect will be decreased. Based on the results presented in this study, it is concluded that the circular pore stack is the thermoacoustic stack geometry that cannot well create the cold-end temperature compared to other geometries, which also includes the groups of the hollow stack such as square pores and honeycomb, which have poor performance, which is in agreement with the Rott functions, as mentioned in section 2. Since the only possibility of these hollow stacks is $\delta_k = \delta_v$, a large radius of hollow pores will cause a ratio of δ_k/δ_v to become zero, and this will not be good with cold-end temperature of hollow stack type.

5 Conclusion

In this study, the experimental and simulation investigations using DeltaEC software are carried out to examine the thermal response of stack geometry and operating mean pressure on the cold end temperature of thermoacoustic stacks. Three different stacks, i.e., spiral, pin array, and circular pore stacks, are built and tested for cold-end temperature on stack. A novel circular pore stack was developed for use in the study. The results of this study show that the operating mean pressure of gas in the system has a greater influence on the cold end temperature of the stack. A high mean pressure of the gas in the system results in a low cold end temperature of stacks due to the large pressure amplitude generated. The cold end temperature reduced to 20.3% for the spiral stack, and 12.7% for the circular pore stack at a pressure of 3 bar. For the pin array, the cold end temperature reduced to 72% at a pressure of 1 bar; these results were compared to the initial temperature. However, increasing the mean pressure should be suitable and correspond to the thermal penetration depth and stack plate spacing. The resulting measurements and simulations indicate that the pin array stack geometry has better cold-end

temperature than the other geometries in terms of the cold end temperature of the stacks. The cold end temperature of the pin array stack is lower than that of the spiral stack and circular pore stack geometry by approximately 63% and 70%, respectively. Unfortunately, the pin array stack has more limited conditions and is more difficult to manufacture than the other geometries. Based on the results of this study, it is concluded that the parallel plate or spiral stack geometry is more suitable for the best performance of thermoacoustic refrigerators. However, to extend the explanation of the influence of both the stack geometry and the mean pressure on the coefficient of the performance *COP* of a refrigerator, the optimum heat exchangers should be installed and analyzed further.

References

1. Swift GW (1988) Thermoacoustic engines. J Acoust Soc Am 84(4): 1145–1180. https://doi.org/10.1121/1.396617
2. Garrett SL, Adeff JA, Hofler TJ (1993) Thermoacoustic refrigerator for space applications. J Thermophys Heat Transf 7(4):595–599. https://doi.org/10.2514/3.466
3. Harris DA, Volkert RE (1989) Design and calibration of an electrodynamic driver for the Space Thermoacoustic Refrigerator (STAR). Master's Thesis, Naval Postgraduate School, Monterey, California
4. Wetzel M, Herman C (1997) Design optimization of thermoacoustic refrigerators. Int J Refrig 20(1):3–21. https://doi.org/10.1016/S0140-7007(96)00064-3
5. Tijani MEH, Zeegers JCH, de Waele ATAM (2002) Design of thermoacoustic refrigerators. Cryogenics 42(1):49–57. https://doi.org/10.1016/s0011-2275(01)00179-5
6. Zolpakar NA, Mohd-Ghazali N, Ahmad R (2016) Experimental investigations of the performance of a standing wave thermoacoustic refrigerator based on multi-objective genetic algorithm optimized parameters. Appl Therm Eng 100:296–303. https://doi.org/10.1016/j.applthermaleng.2016.02.028
7. Wantha C, Assawamartbunlue K (2013) Experimental investigation of the effects of driver housing and resonance tube on the temperature difference across a thermoacoustic stack. Heat Mass Transf 49(6):887–896. https://doi.org/10.1007/s00231-013-1150-y
8. Piccolo A (2011) Numerical computation for parallel plate thermoacoustic heat exchangers in standing wave oscillatory flow. Int J Heat Mass Transf 54(21–22):4518–4530. https://doi.org/10.1016/j.ijheatmasstransfer.2011.06.027
9. Akhavanbazaz M, Siddiqui MHK, Bhat RB (2007) The impact of gas blockage on the performance of a thermoacoustic refrigerator. Exp Thermal Fluid Sci 32(1):231–239. https://doi.org/10.1016/j.expthermflusci.2007.03.009
10. Paek I, Braun JE, Mongeau L (2007) Evaluation of standing-wave thermoacoustic cycles for cooling applications. Int J Refrig 30(6): 1059–1071. https://doi.org/10.1016/j.ijrefrig.2006.12.014
11. Tijani MEH, Zeegers JCH, de Waele ATAM (2002) The optimal stack spacing for thermoacoustic refrigeration. J Acoust Soc Am 112(1):128–133. https://doi.org/10.1121/1.1487842
12. Nsofor EC, Ali A (2009) Experimental study on the performance of the thermoacoustic refrigerating system. Appl Therm Eng 29(13): 2672–2679. https://doi.org/10.1016/j.applthermaleng.2008.12.036
13. Tasnim SH, Mahmud S, Fraser RA (2012) Effects of variation in working fluids and operating conditions on the performance of a thermoacoustic refrigerator. Int Commun Heat Mass Transfer 39(6): 762–768. https://doi.org/10.1016/j.icheatmasstransfer.2012.04.013
14. Arnott WP, Bass HE, Raspet R (1991) General formulation of thermoacoustics for stacks having arbitrarily shaped pore cross sections. J Acoust Soc Am 90(6):3228–3237. https://doi.org/10.1121/1.401432
15. Swift GW (2001) Thermoacoustics: a unifying perspective for some engines and refrigerators, vol Fifth draft. Fifth draft edn. Condensed matter and thermal physics group, Los Alamos National Laboratory
16. Holman J (2011) Experimental Methods for Engineers. McGraw-Hill Education, Boston
17. Keolian RM, Swift GW (1995) Pin stack array for thermoacoustic energy conversion. 5456082, 10/10/1995
18. Nessler FS (1994) Comparison of a pin stack to a conventional stack in a thermoacoustic prime mover. Master's Thesis, Naval Postgraduate School, Monterey, California